Schizosacharomyces pombe RNA polymerase II at 3.6-Å resolution

Henrik Spåhr[1], Guillermo Calero[2], David A. Bushnell, and Roger D. Kornberg[3]

Department of Structural Biology, Stanford University School of Medicine, Stanford, CA 94305

Contributed by Roger D. Kornberg, April 2, 2009 (sent for review March 20, 2009)

The second structure of a eukaryotic RNA polymerase II so far determined, that of the enzyme from the fission yeast *Schizosaccharomyces pombe*, is reported here. Comparison with the previous structure of the enzyme from the budding yeast *Saccharomyces cerevisiae* reveals differences in regions implicated in start site selection and transcription factor interaction. These aspects of the transcription mechanism differ between *S. pombe* and *S. cerevisiae*, but are conserved between *S. pombe* and humans. Amino acid changes apparently responsible for the structural differences are also conserved between *S. pombe* and humans, suggesting that the *S. pombe* structure may be a good surrogate for that of the human enzyme.

molecular replacement | X-ray crystallography | yeast

X-ray crystal structures of RNA polymerases from bacteria and Archaea, and of RNA polymerase II (pol II) from the budding yeast *Saccharomyces cerevisiae*, have given insight into the fundamental mechanism of transcription (1–7). The structures are closely similar in the catalytic core of the enzyme, where mobile elements interact with nucleic acids during transcription. The bacterial and *S. cerevisiae* structures differ in the periphery, where the enzymes interact with accessory factors, most notably the general transcription factors and Mediator of eukaryotes. One of the general factors, transcription factor II B (TFIIB), exhibits a degree of conservation with bacterial sigma factor and has a counterpart in Archaea, and a subunit of another general factor, the TATA-binding protein, occurs in Archaea as well, but the remaining general factors and Mediator are unique to eukaryotes.

Conserved elements of the catalytic core include "switch regions" at the base of a swinging clamp, which interact with the DNA–RNA hybrid and downstream DNA during transcription (2, 3) and may be involved in transcription start site determination (8, 9). A so-called "trigger loop" interacts with the substrate nucleoside triphosphate to achieve the high fidelity of transcription (10–14). A "bridge helix" interacts with the coding base in the template strand of the DNA and is believed to play a role in the translocation step of transcription.

Peripheral, more divergent elements of pol II include subunits Rpb4 and Rpb7, which form a dimer protruding from the enzyme surface (15, 16) and may be involved in RNA binding. Nearby lies the C terminus of Rpb1, from which extends a flexible linker, followed by >20 repeats of a 7-aa sequence [the C-terminal domain (CTD)], which interact not only with Mediator but also with capping, splicing, and cleavage/polyadenylation factors during transcription (17).

Pol II is 53% identical in amino acid sequence between *S. cerevisiae* and humans, assuring a high degree of structural similarity. Notable differences in transcription have nevertheless emerged, including differences in promoter structure and interactions with accessory factors. In these respects, the fission yeast *Schizosaccharomyces pombe* more closely resembles the human system. Promoter DNA melting and other properties are more similar between *S. pombe* and human cells (18). The transcription start site is located ≈30 bp downstream of the TATA box in *S. pombe* and humans, whereas it varies from 40 to 120 bp downstream in *S. cerevisiae* (19). TFIIB has been implicated in start site selection (20–23), and human TFIIB can substitute for endogenous TFIIB in *S. pombe*, whereas *S. cerevisiae* TFIIB cannot (24). The Rpb4/Rpb7 dimer is stoichiometric in *S. pombe* and human. In contrast only 20% is bound during exponential phase in *S. cerevisiae* (25).

Structure determination of human pol II has so far been limited to the individual subunits Rpb6 and Rpb8 by NMR and to the Rpb4/Rpb7 dimer by X-ray crystallography (26–28). Inasmuch as the entire human and other mammalian enzymes have resisted attempts at crystallization, the structure of *S. pombe* pol II is of particular interest. It can provide a basis for understanding mammalian pol II transcription, a platform for assembly and structure determination of complexes with accessory factors. We have previously formed 2D crystals of *S. pombe* pol II and obtained electron density maps in projection at low resolution (29). We now report the formation of large single crystals and structure determination by X-ray analysis.

Table 1. Data collection and refinement statistics

Data collection	
Space group	$P2_12_12_1$
Unit cell dimensions	
a, *b*, *c*, Å	163.0, 202.7, 391.2
a, b, g, °	90, 90, 90
Molecules per asymmetric unit	2
Wavelength, Å	0.98
Resolution, Å	50–3.65 (3.85–3.65)
Unique reflections (observed)	138,872 (19,808)
R_{sym}, %	8.5 (60)
$I/\sigma I$	9.0 (1.3)
Completeness, %	96.6 (95.2)
Redundancy	3.2 (2.3)
Refinement	
R_{work}/R_{free}	29.7/32.1
rmsd	
Bond lengths, Å	0.008
Bond angles, °	1.117

Values in parentheses are for highest-resolution shell.

Results

S. pombe pol II crystallized in space group $P2_12_12_1$ with 2 molecules in the asymmetric unit. The structure was solved by

Author contributions: H.S. designed research; H.S. and G.C. performed research; H.S., G.C., and D.A.B. analyzed data; and H.S. and R.D.K. wrote the paper.

The authors declare no conflict of interest.

Freely available online through the PNAS open access option.

Data deposition: The atomic coordinates have been deposited in the Protein Data Bank, www.pdb.org (PDB ID code 3H0G).

[1]Present address: Department of Laboratory Medicine, Division of Metabolic Diseases, Karolinska Institutet, Novum, SE-141 86 Stockholm, Sweden.

[2]Present address: Department of Structural Biology, University of Pittsburgh Medical School, 1040 Biomedical Science Tower 3 (BST3), 3501 5th Avenue, Pittsburgh, PA 15260.

[3]To whom correspondence should be addressed. E-mail: kornberg@stanford.edu.

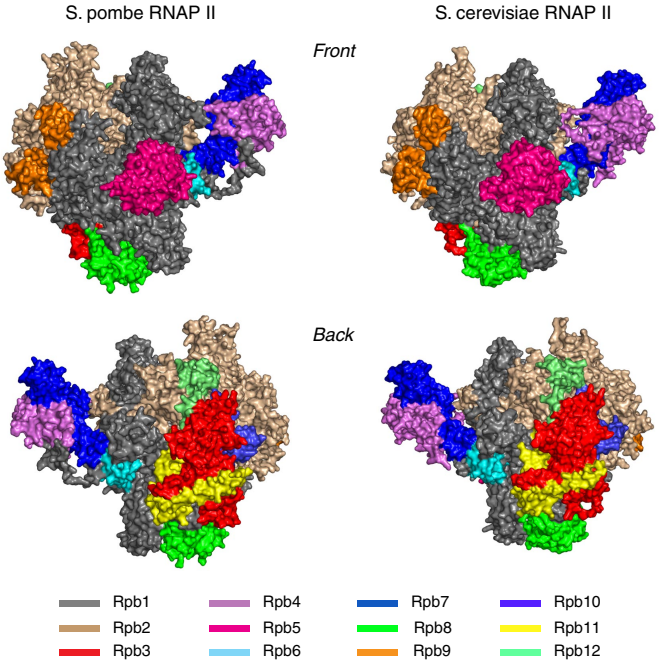

Fig. 1. Structures of pol II from *S. pombe* (*Left*) and *S. cerevisiae* (*Right*, PDB ID code 1WCM). Surface representation of front (*Upper*) and back (*Lower*) views shown. Individual subunits are colored as indicated (2).

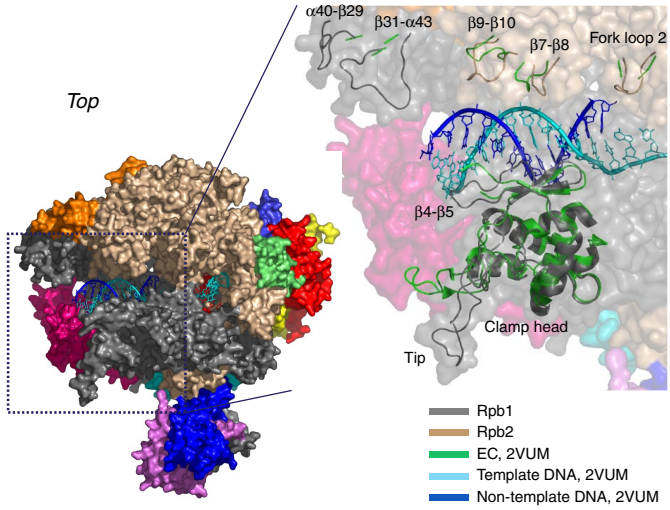

Fig. 2. Structural differences between *S. pombe* and *S. cerevisiae* pol II in the vicinity of the DNA-binding cleft. (*Left*) A surface representation of a top view is shown. (*Right*) The portion in the dashed window in *Left* is enlarged. Colors of Rpb1 and Rpb2 are as in Fig. 1. Template DNA strand in cyan, nontemplate DNA strand in blue, and Rpb1 and Rpb2 loops in green are from an *S. cerevisiae* transcribing complex structure containing α-amanitin (PDB ID code 2VUM), superimposed by aligning Cα atoms of Rpb1 by the secondary structure multiple alignment (SSM) method. Numbering of secondary structure elements in this and subsequent figures is based on *S. cerevisiae* structures as described (2, 45).

molecular replacement with that of *S. cerevisae* pol II, followed by alternating rigid body and translation, libration, and screw rotation displacement (TLS) refinement and manual rebuilding to a final R_{free} of 32.1% (Table 1 and Fig. 1). There were significant differences between the *S. pombe* and *S. cerevisiae* structures in the cleft between Rpb1 and Rpb2, where downstream DNA is located in a transcribing complex (3). On the Rpb1 side of the cleft, loops β31–α43 and α40–β29 were ordered in the *S. pombe* structure. Loop β31–α43 extended far enough

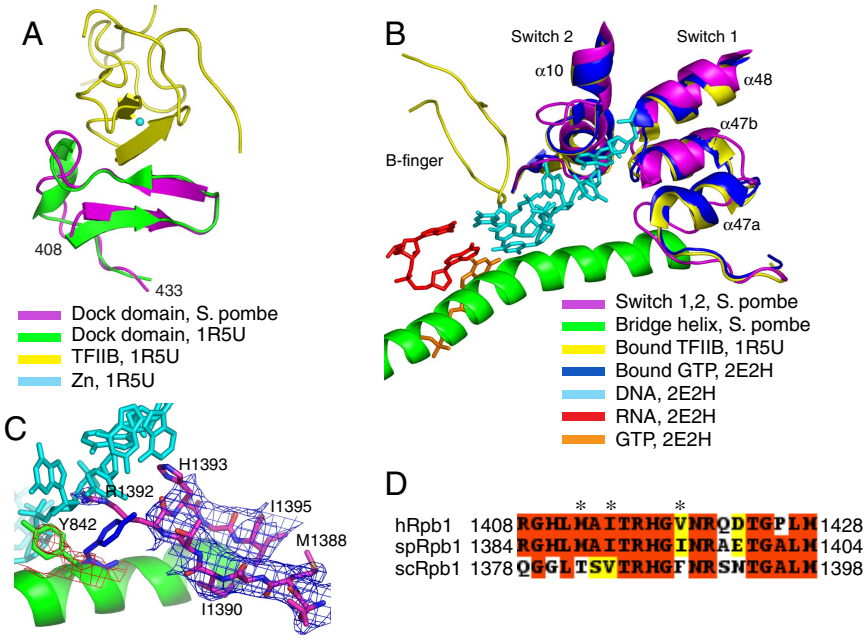

Fig. 3. Dock domain and switch regions. (*A*) Dock domains of *S. pombe* and *S. cerevisiae* from a cocrystal structure with TFIIB (PDB ID code 1R5U) aligned on Cα atoms using the least-squares fit (LSQ) method. (*B*) Switch 1 and 2 regions of *S. pombe*, an *S. cerevisiae* transcribing complex containing GTP in the nucleotide addition site (PDB ID code 2E2H), and an *S. cerevisiae* cocrystal structure with TFIIB (PDB ID code 1R5U) were aligned on Cα atoms using the SSM method. (*C*) *S. pombe* switch 1 loop. A $2F_o - F_c$ map with switch 1 omitted, contoured at 0.9 σ, is shown in blue mesh. The side chain of bridge helix Tyr-842 in *S. pombe* is shown in green, and the same side chain in an *S. cerevisiae* transcribing complex containing GTP in the nucleotide addition site (PDB ID code 2E2H) is shown in blue. A $F_o - F_c$ map with the bridge helix omitted, contoured at 2.2 σ, is shown in red mesh. (*D*) Sequence alignment of the switch 1 loop. Sequences were aligned by using Muscle (46) and colored for conservation in MACBOXSHADE. Asterisks indicate residues conserved or similar to human that appear to stabilize the switch 1 loop conformation.

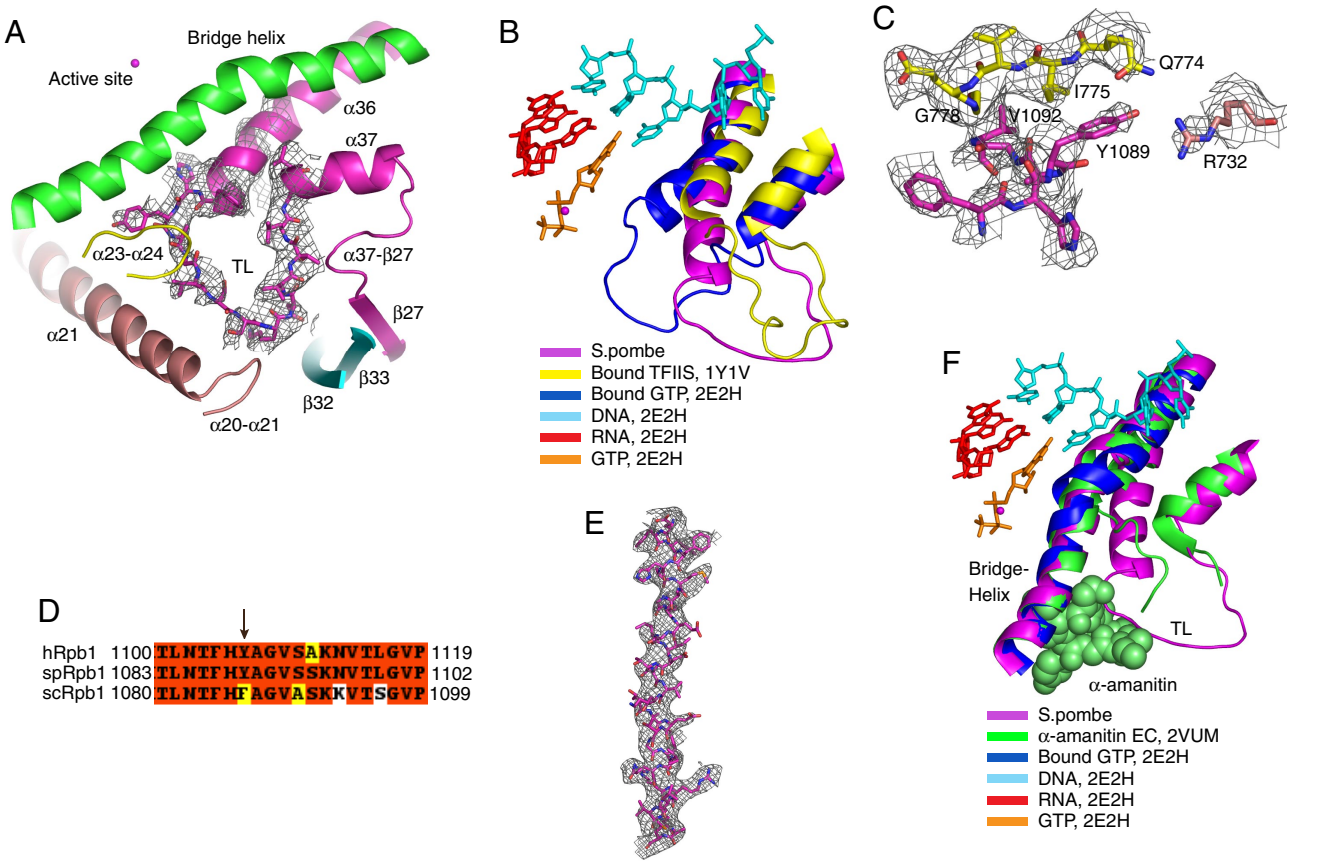

Fig. 4. Trigger loop and bridge helix. (*A*) *S. pombe* trigger loop (TL) depicted as molecular model, and 2 $F_o - F_c$ omit map with trigger loop omitted, contoured at 0.8 σ, shown in gray mesh. Mg^{2+} ion marking the active site is shown as a magenta sphere. (*B*) Trigger loops from *S. pombe*, an *S. cerevisiae* transcribing complex containing GTP in the nucleotide addition site (PDB ID code 2E2H), and an *S. cerevisiae* cocrystal with TFIIS (PDB ID code 1Y1V), aligned on Cα atoms in the bridge helix using the LSQ method. Template DNA, RNA, and GTP are from the *S. cerevisiae* transcribing complex (PDB ID code 2E2H). (*C*) Trigger loop interactions. Trigger loop is in magenta, Rpb1 α23–α24 loop is in yellow, and Rpb1 Arg-732 is in salmon. A 2 $F_o - F_c$ map with all residues indicated omitted, contoured at 0.8 σ, is shown in gray mesh. (*D*) Sequence alignment of the trigger loop as in Fig. 3. Arrow indicates Tyr-1089 conserved between *S. pombe* and human. (*E*) *S. pombe* bridge helix is shown in magenta and a $F_o - F_c$ omit map with bridge helix omitted, contoured at 2.5 σ, is shown in gray mesh. (*F*) Bridge helices in *S. pombe*, an *S. cerevisiae* transcribing complex containing GTP in the nucleotide addition site (PDB ID code 2E2H), and an *S. cerevisiae* transcribing complex containing α-amanitin (PDB ID code 2VUM), were aligned on Cα atoms using the LSQ method. Green spheres represent α-amanitin.

for possible contact with the downstream DNA. The Rpb1 "clamp head," which can be cross-linked to TFIIE in *S. cerevisiae* (30), adopted a different conformation in *S. pombe* (Fig. 2). Loop β4–β5, only partially ordered in *S. cerevisiae*, could be built in *S. pombe*, and its position, together with a shift of ≈15 Å of the clamp head tip, resulted in a more open conformation. On the Rpb2 side of the cleft, a series of loops protruding from the "lobe" domain had different conformations in *S. pombe*. Loop β9–β10, which can be cross-linked to TFIIF in *S. cerevisiae* (30), and loop β7–β8 were shifted toward downstream DNA in *S. pombe*. Fork loop 2, only seen in its entirety in *S. cerevisiae* after an advanced refinement approach (31), could be completely built in *S. pombe*, in a location where it would block the path of the nontemplate DNA strand in a transcribing complex, and thus contribute to the formation of the downstream edge of the transcription bubble (3, 32).

Another difference in surface conformation was in the Rpb1 "dock domain," where TFIIB was bound in a previous cocrystal with pol II (20). A helix in *S. cerevisiae* adopted a loop conformation in *S. pombe* that was shifted in the direction of TFIIB (Fig. 3*A*). His-424$^{Ser\text{-}418}$ (*S. cerevisiae* residue in superScript) in the tip of the loop, in close proximity to TFIIB, is conserved in humans, but replaced by a serine in *S. cerevisiae*.

Switches 1 and 2. Whereas Rpb1 switches 1 and 2 were only ordered in the presence of DNA and RNA in an *S. cerevisiae*-transcribing complex (3), both switches were well ordered in the *S. pombe* structure (Fig. 3*B*). A short helix in switch 1, α47a, adopted a loop conformation in *S. pombe*, pointing toward the location of DNA in the transcribing complex (Fig. 3*C*). This conformation was made possible by movement of Tyr-842$^{Tyr\text{-}836}$ of the bridge helix and was stabilized by Met-1388$^{Thr\text{-}1382}$, Ile-1390$^{Val\text{-}1384}$, and Ile-1395$^{Phe\text{-}1389}$, which positioned Arg-1392$^{Arg\text{-}1386}$ and His-1393$^{His\text{-}1387}$ for DNA contact (Fig. 3*C*). The stabilizing residues are conserved in human pol II, but differ in *S. cerevisiae* (Fig. 3*D*).

In switch 2, 4 residues in the middle of α-helix 10 were flipped out and shifted ≈4.5 Å, compared with all *S. cerevisiae* structures (Fig. 3*B*). The flipped-out region was in close proximity to the B finger in the pol II–TFIIB cocrystal structure (20) and contained the conserved residue Lys-338$^{Lys\text{-}332}$ shown to shift the transcription start site downstream upon mutation in *S. cerevisiae* (9). Mutations in switch 1 have been shown to shift the transcription start site downstream as well (8).

Trigger Loop and Bridge Helix. Continuous density was observed for the entire Rpb1 trigger loop in the *S. pombe* structure (Fig. 4*A*). In contrast, continuous density was only observed for the trigger loop in *S. cerevisiae* in a transcribing complex (13) or in the presence of TFIIS (32). The conformation in *S. pombe* was

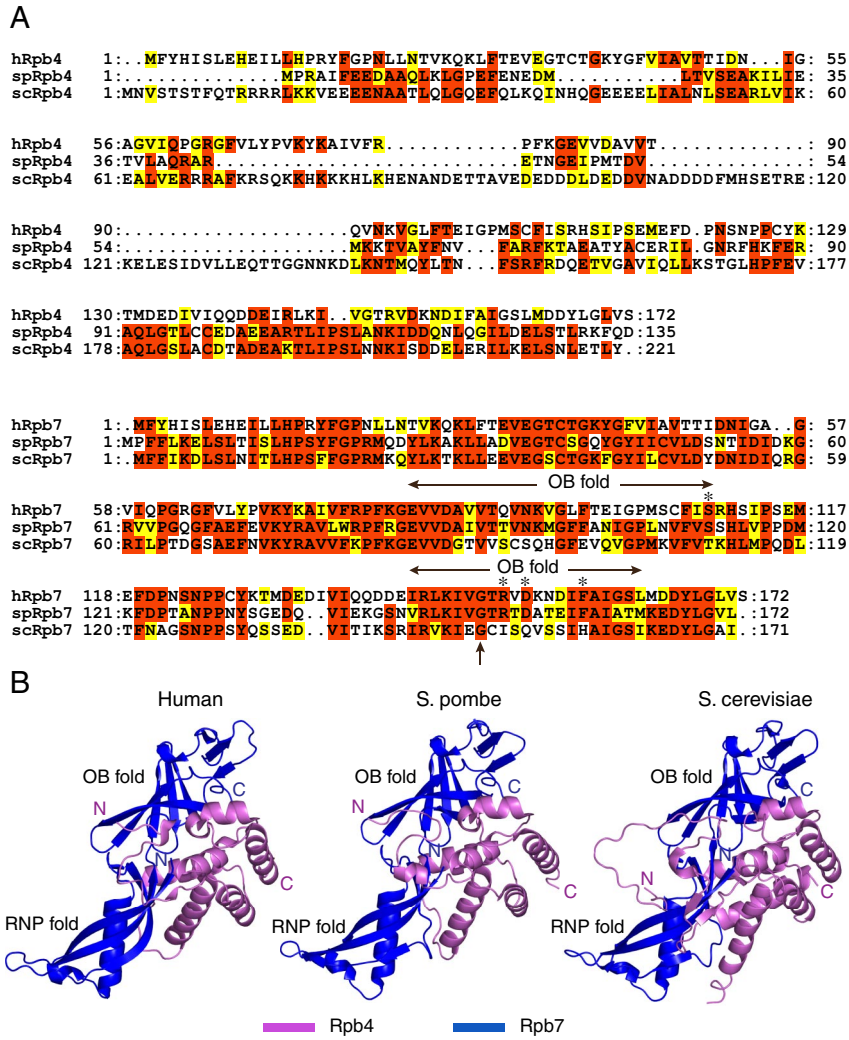

Fig. 5. Rpb4/Rpb7 dimer. (*A*) Sequence alignments of Rpb4 and Rpb7 are as in Fig. 3. Mutations in human within the OB fold that decrease RNA binding are indicated by asterisks, and the temperature-sensitive G150D mutation is indicated by an arrow. (*B*) Structures of the Rpb4/Rpb7 dimer from human PDB ID code 2C35, *S. pombe* and *S. cerevisiae* PDB ID code 1WCM. The RNA-binding OB and RNP folds and the N and C termini of Rpb4 and Rpb7 are indicated.

intermediate between those in the 2 previous *S. cerevisiae* structures (Fig. 4*B*). The *S. pombe* conformation was stabilized by interactions with the bridge helix and Rpb1 loop α23–α24, helix α21, strand β32, strand β33, loop α20–α21, and loop α37–β27. Helix α36, immediately adjacent to the trigger loop, was 1 turn longer in the *S. pombe* structure. Tyr-1089$^{\text{Phe-1086}}$ of the trigger loop made contacts with Rpb1 residues Glu-774$^{\text{Glu-768}}$, Ile-775$^{\text{Ser-769}}$, and Arg-732$^{\text{Arg-726}}$ (Fig. 4 *C* and *D*). An additional contact was formed between Val-1092$^{\text{Val-1089}}$ of the trigger loop and Rpb1 residue Gly-778$^{\text{Gly-772}}$. Tyr-1089$^{\text{Phe-1086}}$ is conserved in humans, but replaced by a phenylalanine in *S. cerevisiae*; indeed, the entire trigger loop sequence is more similar between *S. pombe* and humans than between either and *S. cerevisiae* (Fig. 4*D*).

The bridge helix was helical along its entire length (Fig. 4*E*), with a kink at a position previously seen in an *S. cerevisiae* transcribing complex in the presence of α-amanitin (33), and shifted 1 turn with respect to a transcribing complex with bound GTP (13). The kink in the presence of α-amanitin was apparently stabilized by the trigger loop wedged between Rpb1 helix α37 and the bridge helix (33). In *S. pombe*, however, the kink was observed in the same position despite a different location of the trigger loop (Fig. 4*F*). Binding of α-amanitin in *S. pombe* would be expected to disrupt interaction between the trigger loop and Rpb1 loop α23–α24 and prevent swinging of the trigger loop into the active site to facilitate transcription.

Rpb4/Rpb7 Dimer. The sequence similarity of Rpb7 among *S. pombe*, *S. cerevisiae*, and humans was high, whereas the sequence similarity of Rpb4 was considerably lower (Fig. 5*A*). The structure of the Rpb4/Rpb7 dimer showed a greater similarity of *S. pombe* to human than to *S. cerevisiae* (Fig. 5*B*). Indeed, Rpb4 was highly similar in structure in *S. pombe* and human despite the low sequence conservation. Two central insertions present in *S. cerevisiae* were absent, one containing 11 residues, with a pair of short antiparallel β-strands, and a second insertion that in *S. cerevisiae* contains a 15-residue helix and a flexible unbuilt region, replaced in *S. pombe* and humans by a loop between helices H1 and H2. The Rpb4/Rpb7 dimer was linked to the rest of pol II through contacts of the N-terminal domain of Rpb7 with Rpb1 and Rpb6 (Fig. 6). Contacts made by the variable N-terminal region of Rpb4 in *S. cerevisiae*, 14 residues shorter in *S. pombe*, were lacking.

Rpb7 contains 2 RNA binding motifs, an OB fold and a RNP fold, conserved in eukaryotes and Archaea (16, 28, 34). Mutagenesis of the OB fold of human Rpb7 has implicated Ser-109, Arg-151, Asp-153, and Phe-158 in RNA binding (28). These

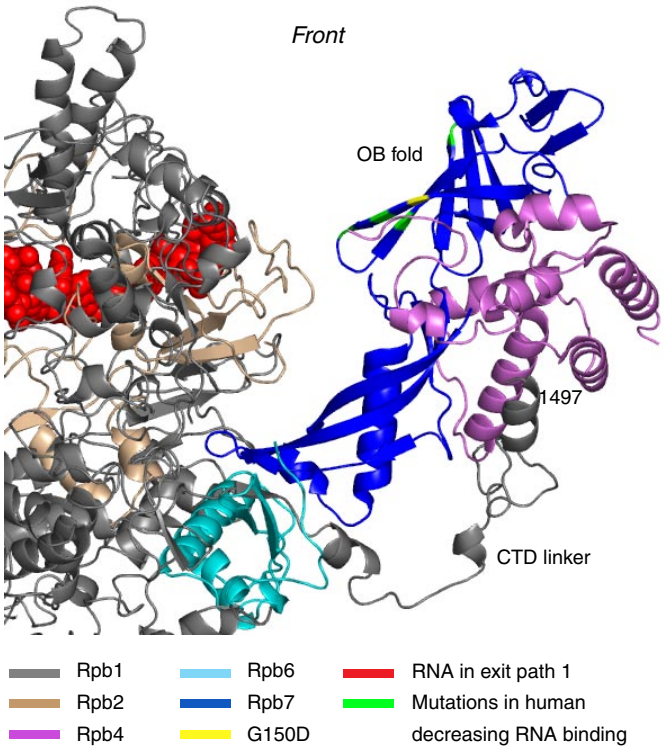

Fig. 6. Rpb4/Rpb7 interactions with other pol II subunits. Front view of pol II is shown. Mutations in human within the OB fold that decrease RNA binding are indicated in green and the temperature-sensitive G150D mutation is indicated in yellow. RNA exit path 1 is from ref. 1.

residues are all conserved in *S. pombe* (Ser-112$^{\text{Thr-111}}$, Arg-152$^{\text{Ile-151}}$, Asp-154$^{\text{Glu-153}}$, and Phe-159$^{\text{His-158}}$), but not in *S. cerevisiae* (Fig. 5*A*). They are located adjacent to RNA as it exits the enzyme (Fig. 6). A mutation in the same region of the *S. pombe* enzyme, G150D$^{\text{G 149}}$ (Figs. 5*A* and 6), almost abolished transcriptional activity at an elevated temperature (35).

CTD Linker. The last ordered residue of *S. cerevisiae* Rpb1 was Leu-1450, whereas the *S. pombe* chain could be traced as far as residue 1497 (Fig. 6). The additional ordered region, which forms part of the linker to the CTD, included a short central helix, followed by a loop stabilized by contact with Rpb4 loop H1–H2. Helix H1, ≈1½ turns shorter in *S. pombe* and humans than in *S. cerevisiae*, provided a further interaction surface for the linker and contacts with Rpb4 helix H3 were seen as well. Because of crystal packing differences, residues 1460–1490 of the second molecule in the asymmetric unit were too flexible for model building, but clear density for the linker extended to residue 1506, where an additional helix was observed.

Discussion

S. pombe and *S. cerevisiae* differ in the distance from the TATA box to the start site of pol II transcription. Structural differences between the 2 polymerases reported here may be responsible. These differences lie along the path of the DNA in the transcribing enzyme and in sites of interaction with general transcription factors involved in transcription initiation. Where DNA enters the pol II cleft, 3 loops, Rpb1 β4–β5, β31–α43, and α40–β29, become structured in *S. pombe*, resulting in a different interface for binding the general factors TFIIE and TFIIH, proposed to interact in this region (20, 30). In addition, 2 loops in the Rpb2 lobe domain, β7–β8 and β9–β10, are shifted toward downstream DNA, which may affect pol II binding to TFIIF. Further along the cleft, the switch regions, important for binding the DNA–RNA hybrid, and start site selection (3, 8, 9), are structured in the absence of DNA in *S. pombe*, but not in *S. cerevisiae*. TFIIB, also important for start site selection, interacts with the pol II dock domain, which differs in structure between *S. pombe* and *S. cerevisiae* as well.

S. pombe pol II displays additional structured regions not observed in the *S. cerevisiae* enzyme. The CTD linker could be seen in *S. pombe* pol II following a path along Rpb4 toward the OB fold of Rpb7, which may bind RNA as it exits from the enzyme. The trigger loop was also seen in its entirety in the free enzyme, whereas it was only fully structured in *S. cerevisiae* in a transcribing complex in the presence of nucleoside triphosphate.

Amino acid residues important for these structural differences between *S. pombe* and *S. cerevisiae* are conserved between *S. pombe* and humans. Residues stabilizing switch 1, residues of the trigger loop, and residues in the OB fold all exhibit such conservation. Because *S. pombe* resembles the human system in start site location and other respects, this conservation further suggests that functional differences with the *S. cerevisiae* system are caused by the structural differences observed. The conservation also indicates the value of the *S. pombe* pol II structure as a model for the human enzyme.

Materials and Methods

Preparation and Crystallization of Pol II. *S. pombe* pol II was purified as described (36) and concentrated to 11 mg/mL with change of buffer to 10 mM Tris·HCl (pH 7.5), 25 mM KCl, 0.1 mM EDTA, 1 μM $ZnCl_2$, 10 mM DTT. Crystals were grown at 16 °C by the sessile drop- vapor diffusion method, by adding pentaethylene glycol monooctyl ether (C8E5) to 1.2 μL of protein at a final concentration of 14.2 mM and mixing with an equal volume of reservoir solution [50 mM Mes (pH 6.3), 300 mM ammonium acetate, 5–6.5% (wt/vol) polyethylene glycol (PEG) 4000, and 10 mM DTT]. After 9 days, crystals were crushed and microseeded into a fresh drop prepared as before except with Mes, pH 6.6, and 3.6% PEG 4000. After several rounds of microseeding, long rod-shaped crystals (0.1 × 0.1 × 0.6 mm) were obtained. The crystals were harvested by transfer in 2 steps over 1 h to mother liquor containing 15–30% glycerol and cryo-coded in liquid nitrogen.

Data Collection and Processing. Diffraction data were collected at the Stanford Radiation Laboratory (Menlo Park, CA) on beamlines 11-1 and 9-2, and at the Advanced Light Source, Lawrence Berkeley National Laboratory (Berkeley, CA) on beamlines 5.0.2 and 8.2.2. Data were processed with MOSFLM (37) and SCALA (38). The structure was solved by molecular replacement with Phaser (39), using 12-subunit pol II from *S. cerevisiae* as search model [Protein Data Bank (PDB) ID code 1WCM]. The molecular replacement solution was subjected to rigid body refinement with CNS (40) and prime and switch density modification including noncrystallographic symmetry (NCS) with Resolve to remove model bias (41). An initial $2F_o - F_c$ map was used for manual fitting and model building in Coot (42). The improved model was subjected to bulk solvent correction, rigid body, group ADP, and TLS refinement with automatic NCS using Phenix (43, 44). Strict NCS was used during all refinement steps after the model built in molecule 1 had been transferred to molecule 2, with the exception of the CTD linker that showed differences in the 2 molecules. After several rounds of manual model building and refinement in Phenix, the final free *R* factor was lowered to 32.1%. Figures were prepared with Pymol (http://pymol.sourceforge.net).

ACKNOWLEDGMENTS. We thank C. Kaplan, K. M. Larsson, and R. Davis for advice and assistance. H.S. was supported by a Marie Curie Outgoing International Fellowship, funded by the European Commission under the sixth framework program (Contract 8574). Part of the research was carried out at the Stanford Synchrotron Radiation Laboratory and the Advanced Light Source. The Stanford Synchrotron Radiation Laboratory structural biology program is supported by the Department of Energy, Office of Biological and Environmental Research, the National Institutes of Health, National Center for Research Resources, Biomedical Technology Program, and the National Institute of General Medical Sciences. The Advanced Light Source is operated by Lawrence Berkeley National Laboratory and is supported in part by the Department of Energy, Office of Biological and Environmental Research, and the National Institutes of Health, National Institute of General Medical Sciences. This work was supported by National Institutes of Health Grant GM49985 (to R.D.K.).

1. Cramer P, et al. (2000) Architecture of RNA polymerase II and implications for the transcription mechanism. *Science* 288:640–649.
2. Cramer P, Bushnell DA, Kornberg RD (2001) Structural basis of transcription: RNA polymerase II at 2.8-Å resolution. *Science* 292:1863–1876.
3. Gnatt AL, Cramer P, Fu J, Bushnell DA, Kornberg RD (2001) Structural basis of transcription: An RNA polymerase II elongation complex at 3.3-Å resolution. *Science* 292:1876–1882.
4. Murakami KS, Masuda S, Campbell EA, Muzzin O, Darst SA (2002) Structural basis of transcription initiation: An RNA polymerase holoenzyme–DNA complex. *Science* 296:1285–1290.
5. Murakami KS, Masuda S, Darst SA (2002) Structural basis of transcription initiation: RNA polymerase holoenzyme at 4-Å resolution. *Science* 296:1280–1284.
6. Vassylyev DG, et al. (2002) Crystal structure of a bacterial RNA polymerase holoenzyme at 2.6-Å resolution. *Nature* 417:712–719.
7. Zhang G, et al. (1999) Crystal structure of *Thermus aquaticus* core RNA polymerase at 3.3-Å resolution. *Cell* 98:811–824.
8. Kwapisz M, et al. (2008) Mutations of RNA polymerase II activate key genes of the nucleoside triphosphate biosynthetic pathways. *EMBO J* 27:2411–2421.
9. Majovski RC, Khaperskyy DA, Ghazy MA, Ponticelli AS (2005) A functional role for the switch 2 region of yeast RNA polymerase II in transcription start site utilization and abortive initiation. *J Biol Chem* 280:34917–34923.
10. Kaplan CD, Larsson KM, Kornberg RD (2008) The RNA polymerase II trigger loop functions in substrate selection and is directly targeted by α-amanitin. *Mol Cell* 30:547–556.
11. Vassylyev DG, Vassylyeva MN, Perederina A, Tahirov TH, Artsimovitch I (2007) Structural basis for transcription elongation by bacterial RNA polymerase. *Nature* 448:157–162.
12. Vassylyev DG, et al. (2007) Structural basis for substrate loading in bacterial RNA polymerase. *Nature* 448:163–168.
13. Wang D, Bushnell DA, Westover KD, Kaplan CD, Kornberg RD (2006) Structural basis of transcription: Role of the trigger loop in substrate specificity and catalysis. *Cell* 127:941–954.
14. Westover KD, Bushnell DA, Kornberg RD (2004) Structural basis of transcription: Nucleotide selection by rotation in the RNA polymerase II active center. *Cell* 119:481–489.
15. Armache KJ, Kettenberger H, Cramer P (2003) Architecture of initiation-competent 12-subunit RNA polymerase II. *Proc Natl Acad Sci USA* 100:6964–6968.
16. Bushnell DA, Kornberg RD (2003) Complete, 12-subunit RNA polymerase II at 4.1-Å resolution: Implications for the initiation of transcription. *Proc Natl Acad Sci USA* 100:6969–6973.
17. Pandit S, Wang D, Fu XD (2008) Functional integration of transcriptional and RNA processing machineries. *Curr Opin Cell Biol* 20:260–265.
18. Choi WS, Lin YC, Gralla JD (2004) The *Schizosaccharomyces pombe* open promoter bubble: Mammalian-like arrangement and properties. *J Mol Biol* 340:981–989.
19. Li Y, Flanagan PM, Tschochner H, Kornberg RD (1994) RNA polymerase II initiation factor interactions and transcription start site selection. *Science* 263:805–807.
20. Bushnell DA, Westover KD, Davis RE, Kornberg RD (2004) Structural basis of transcription: An RNA polymerase II-TFIIB cocrystal at 4.5 Å. *Science* 303:983–988.
21. Hawkes NA, Roberts SG (1999) The role of human TFIIB in transcription start site selection in vitro and in vivo. *J Biol Chem* 274:14337–14343.
22. Pardee TS, Bangur CS, Ponticelli AS (1998) The N-terminal region of yeast TFIIB contains two adjacent functional domains involved in stable RNA polymerase II binding and transcription start site selection. *J Biol Chem* 273:17859–17864.
23. Pinto I, Wu WH, Na JG, Hampsey M (1994) Characterization of sua7 mutations defines a domain of TFIIB involved in transcription start site selection in yeast. *J Biol Chem* 269:30569–30573.
24. Choi WS, Yan M, Nusinow D, Gralla JD (2002) In vitro transcription and start site selection in *Schizosaccharomyces pombe*. *J Mol Biol* 319:1005–1013.
25. Choder M, Young RA (1993) A portion of RNA polymerase II molecules has a component essential for stress responses and stress survival. *Mol Cell Biol* 13:6984–6991.
26. del Rio-Portilla F, Gaskell A, Gilbert D, Ladias JA, Wagner G (1999) Solution structure of the hRPABC14.4 subunit of human RNA polymerases. *Nat Struct Biol* 6:1039–1042.
27. Kang X, et al. (2006) Structural, biochemical, and dynamic characterizations of the hRPB8 subunit of human RNA polymerases. *J Biol Chem* 281:18216–18226.
28. Meka H, Werner F, Cordell SC, Onesti S, Brick P (2005) Crystal structure and RNA binding of the Rpb4/Rpb7 subunits of human RNA polymerase II. *Nucleic Acids Res* 33:6435–6444.
29. Meredith G (1998) Structural features of yeast RNA polymerase II via electron crystallography. Thesis (Stanford University, Stanford, CA).
30. Chen HT, Warfield L, Hahn S (2007) The positions of TFIIF and TFIIE in the RNA polymerase II transcription preinitiation complex. *Nat Struct Mol Biol* 14:696–703.
31. Meyer PA, Ye P, Suh MH, Zhang M, Fu J (2009) Structure of the 12-subunit RNA polymerase II refined with the aid of anomalous diffraction data. *J Biol Chem* 284:12933–12939.
32. Kettenberger H, Armache KJ, Cramer P (2004) Complete RNA polymerase II elongation complex structure and its interactions with NTP and TFIIS. *Mol Cell* 16:955–965.
33. Brueckner F, Cramer P (2008) Structural basis of transcription inhibition by α-amanitin and implications for RNA polymerase II translocation. *Nat Struct Mol Biol* 15:811–818.
34. Todone F, Brick P, Werner F, Weinzierl RO, Onesti S (2001) Structure of an archaeal homolog of the eukaryotic RNA polymerase II RPB4/RPB7 complex. *Mol Cell* 8:1137–1143.
35. Djupedal I, et al. (2005) RNA Pol II subunit Rpb7 promotes centromeric transcription and RNAi-directed chromatin silencing. *Genes Dev* 19:2301–2306.
36. Banks CA, et al. (2007) Identification and characterization of a *Schizosaccharomyces pombe* RNA polymerase II elongation factor with similarity to the metazoan transcription factor ELL. *J Biol Chem* 282:5761–5769.
37. Powell HR (1999) The Rossmann Fourier autoindexing algorithm in MOSFLM. *Acta Crystallogr D* 55:1690–1695.
38. Potterton E, McNicholas S, Krissinel E, Cowtan K, Noble M (2002) The CCP4 molecular-graphics project. *Acta Crystallogr D* 58:1955–1957.
39. McCoy AJ, Grosse-Kunstleve RW, Storoni LC, Read RJ (2005) Likelihood-enhanced fast translation functions. *Acta Crystallogr D* 61:458–464.
40. Brunger AT, et al. (1998) Crystallography and NMR system: A new software suite for macromolecular structure determination. *Acta Crystallogr D* 54:905–921.
41. Terwilliger TC (2000) Maximum-likelihood density modification. *Acta Crystallogr D* 56:965–972.
42. Emsley P, Cowtan K (2004) Coot: Model-building tools for molecular graphics. *Acta Crystallogr D* 60:2126–2132.
43. Adams PD, et al. (2004) Recent developments in the PHENIX software for automated crystallographic structure determination. *J Synchrotron Radiat* 11:53–55.
44. Adams PD, et al. (2002) PHENIX: Building new software for automated crystallographic structure determination. *Acta Crystallogr D* 58:1948–1954.
45. Armache KJ, Mitterweger S, Meinhart A, Cramer P (2005) Structures of complete RNA polymerase II and its subcomplex, Rpb4/7. *J Biol Chem* 280:7131–7134.
46. Edgar RC (2004) MUSCLE: Multiple sequence alignment with high accuracy and high throughput. *Nucleic Acids Res* 32:1792–1797.